Available online at www.sciencedirect.com

ScienceDirect

Procedia CIRP 133 (2025) 656–661

www.elsevier.com/locate/procedia

20th CIRP Conference on Modeling of Machining Operations

Investigation on cutting fluid use in finish milling of polylactide (PLA) 3D-printed parts

Margaux Lorenzoni*[,a], Laurent Spitaels[a], Edouard Rivière-Lorphèvre[a], Jérémy Odent[b], Rachid M'Saoubi[c,d], Liam Cloëz[e], Michaël Fontaine[e], François Ducobu[a]

[a]*Machine Design and Production Engineering Lab – Research Institute for Materials Science and Engineering, University of Mons, Place du Parc 20, 7000 Mons, Belgium*

[b]*Laboratory of Polymeric and Composite Materials (LMPC) – Center of Innovation and Research in Materials and Polymers (CIRMAP), University of Mons, Place du Parc 20, 7000 Mons, Belgium*

[c]*R&D Material and Technology Development, Seco Tools AB, Björnbacksvägen 2, SE-737 82 Fagersta, Sweden*

[d]*Department of Mechanical Engineering Sciences - Division of Production and Materials Engineering, Lund University, Ole Römers väg 1, SE-221 00 Lund, Sweden*

[e]*FEMTO-ST Institute – Applied Mechanics Dept., Université de Franche-Comté – SUPMICROTECH – CNRS, Rue de l'épitaphe 24, F-25000 Besançon, France*

* Corresponding author. *E-mail address:* margaux.lorenzoni@umons.ac.be

Abstract

Fused Filament Fabrication (FFF) is an additive manufacturing process based on Material Extrusion (MEX) of polymeric filament. This manufacturing technology is commonly used for personalized production applications and prototyping, allowing to obtain customized parts with complex geometries at a low cost. However, this production technique has its limitations regarding dimensional accuracy and surface roughness of the final parts. To overcome these limitations, finish milling is considered to be a promising technique as it is widely used for metallic parts. Yet, the specific thermal properties of polymers such as low thermal conductivity and low melting temperature are adding a challenge in the determination of optimal cutting conditions. In this context, the use of cutting fluid could be the key to keep the material from melting during milling. Therefore, this paper proposes to compare the impact of using a compressed air flow to dry conditions on the cutting forces and the surface quality obtained on 3D-printed polylactide (PLA) parts. The qualification test of the tool-material couple standard (NF E 66-520-6) will be used as a guideline to determine the relevance of cutting fluid use for cutting conditions varying around an operating point. Moreover, simulated cutting forces using a mechanistic model will be compared to experimental data to evaluate the applicability of the model.

Keywords: Polylactic acid; PLA; Additive manufacturing; Milling, Finishing; Cutting fluid; Modeling

1. Introduction

1.1. Context

Since its invention in 1988, the Material Extrusion (MEX) process, an Additive Manufacturing (AM) technology, has developed quickly, enabling the manufacturing of complex geometries at a lower cost [1]. This process consists in building a part by adding melted material layer by layer. Fused Filament Fabrication (FFF), a MEX derivative, is particularly friendly for both private users and industries due to its filament feedstock [2]. Furthermore, applications have expanded from modeling and prototyping to small series and personalized production [1].

However, some limitations remain in terms of achieving tight dimensional tolerances and fine surface roughness [2]. Post-processing, like finish milling, is a promising approach to solve these limitations as it shows the best surface finish improvement among mechanical methods [3] as well as improvement in terms of dimensional accuracy [4].

10.1016/j.procir.2025.02.112

Furthermore, it could later be implemented inside of a hybrid structure combining the MEX process and machining [5].

Many polymers can be employed with the MEX process. Yet, few of them are bio sourced and recyclable, which inevitably leads to ecological concerns as the technology is growing. Polylactide or Polylactic acid (PLA) is, to this end, an interesting material as it can be produced from corn, sugar beet or cane, etc. [6] and recycled in different ways as well as composted in the presence of micro-organisms [7,8].

PLA is a semicrystalline thermoplastic constituted of three stereoisomers. Thermal and mechanical properties as well as crystallinity of PLA depend on molecular weight and polymer architecture (proportion of crystalline and amorphous stereoisomers) [8]. It can be produced in two ways leading to different molecular weight. In this study, the name Polylactide is used for PLA since it is produced by catalytic ring-opening and showing a higher molecular weight [8].

1.2. Literature review and motivation of the study

Multiple groups have started to study drilling [9] and milling of PLA [4,10–14]. Different milling operations are studied such as slot milling [10–12], pocket milling [13], profile milling [4] and shoulder milling [14]. Furthermore, studies focus on different aspects of the machining process: cutting forces during milling [10], burr formation [12,13] and arithmetic surface roughness R_a after machining [4,10–12,14].

Regarding surface roughness, the best results are obtained by Lalegani Dezaki et al. [4] reaching a R_a of 0.358 µm. However, different tools are used to machine a complex surface, and it is unclear where this surface quality is obtained. Pămărac and Petruse [14] also reach low surface roughness by achieving a R_a of 0.6 µm in shoulder milling. Overall, the cutting conditions leading to the best surface roughness for each of the previously mentioned studies are synthesized in Table 1, giving the tool diameter D, its number of teeth Z in addition to the cutting speed v_c, the feed per tooth f_z and the axial and radial depth of cut a_p and a_e.

Table 1. Summary of cutting parameters in previous studies.

Study	D [mm]	Z	v_c [m/min]	f_z [mm/tooth]	a_p [mm]	a_e [mm]	CF
[4]	12	4	165	0.057	1	5/12	Air
[10]	6	2	75.4	0.1	2	6	No
[11]	12	4	132	0.086	20	5	Air
[12]	6	2	103.7	0.036	0.2	6	Yes
[13]	10	4	471.2	0.008	0.5	10	Air
[14]	6	2	66	0.155	3	6	Air

Except for Cloëz et al. [10], all studies choose to use a cutting fluid (CF) during machining to ensure proper chip removal and provide a cooling effect on the material. When the CF is specified, pressurized air is mentioned. Indeed, there are different kinds of CF, but cooling liquids are rather avoided due to the lack of information on the interaction between the CF and the material as well as their impact on the environment [13]. However, no studies have been comparing results of machining with or without CF use.

Further studies, such as Dilberoglu et al. [15], insist on the influence of heat generation during machining of polymeric materials. Polymers such as PLA have high thermal expansion coefficients (between 50 and 2000 µm/mK) [16] and, unlike metals, are natural insulators (thermal conductivity λ of 0.12 W/(m.K) for PLA [17] against 237 W/(m.K) for aluminum [18]). Therefore, heat induced by the machining process may be unable to dissipate from the machined zone and may cause the workpiece thermal deformation and/or degradation [16], especially if the glass transition temperature is reached [15].

Regarding burr formation, Mehtedi et al. [12] concludes that higher burr formation is linked to heat generation during machining which can soften material. Therefore, monitoring temperature during milling can be relevant.

Machining of 3D-printed parts requires special considerations regarding the depths of cut. Boschetto et al. [19] recommend setting them to cut through the layers rather than cutting between layers. In this manner, depths of cut are large enough to erase the original morphology of the surface but are not leading to cut into the interlayer zone where internal voids and defects can appear.

As for modeling of cutting forces, literature studies the topic extensively regarding machining of metallic materials [20]. Cutting forces models also exist in literature regarding fiber-reinforced polymeric matrix composites [21] but there are, however, no references for the specific case of polymers, such as PLA, alone. Therefore, using a usual mechanistic model designed for metallic materials such as the one developed by Rivière-Lorphèvre and Filippi [22] seems to be the first approach to investigate.

In summary, some questions are, so far, left unanswered about modeling of PLA machining as well as the impact of CF use on heat generation and dissipation during the machining process. Potential effects of heat rise on surface quality and cutting forces are also to be determined. Therefore, this study aims to determine the relevance of using compressed air as a CF to ensure effective heat dissipation during finish milling of FFF-obtained parts to guarantee low surface roughness of the machined areas and process stability in terms of cutting forces, as well as to evaluate the applicability of a mechanistic model for PLA machining.

2. Material and Method

2.1. Part design and printing

To optimize samples, the parts were cross-shaped to allow shoulder milling operations on each of the cross sides without interfering with other sides. The parts are described in Fig. 1. A fillet of 0.4 mm, equivalent to the nozzle diameter, ensures ease of printing [1].

The parts were printed from 2.85 mm-diameter filament of Native Nanovia EF 3D850 Polylactic Acid (PLA). The material was dried using a SUNLU FilaDryer S2 during 16 hours before printing, reaching a 20% humidity level inside of the drying device. The material thermal properties were determined using Differential Scanning Calorimetry (DSC) on a TA Instruments DSC Q2000. Testing was performed at heating and cooling rates of 10°C/min (according to ISO

11357) between -20°C and 210°C; a second scan was used to avoid any thermal history effects. Transition temperatures were calculated as follows:

- Glass transition temperature T_g: 61°C
- Crystallization temperature T_c: 104°C
- Melting temperature T_m: 176°C

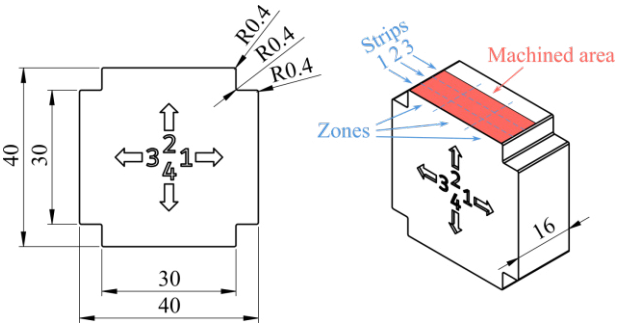

Fig. 1. Design of the parts (in mm) and definition of strips and zones.

The printer used was an Ultimaker S3 with AA 0.4 mm print cores. A light mist of 3DLAC adhesive spray was applied on the build plate before each print to avoid samples warping. Since the parts are meant to be finished by milling, printing parameters were chosen using a modified version (Table 2) of the Balanced Fast printing strategy proposed by the slicer, namely Ultimaker Cura 5.6.0, to match the material manufacturer's recommendation [23].

Table 2. Modified printing parameters.

Printing parameter	Value
Wall thickness	5 mm
Top/Bottom thickness	1 mm
Top/Bottom pattern	Concentric
Infill density	10%
Infill pattern	Grid
Printing temperature	200°C
Print speed	50 mm/s

2.2. Finish milling and cutting conditions

Finish milling operations, with a shoulder milling approach, were performed on a Mikron VCE 600 Pro. When used, the CF was a compressed air flow at a pressure of 6 bar.

The selected tool for this study was the 93060-F solid end mill from Seco Tools specifically designed for thermoplastics. The mill showed a 6 mm-diameter (D) with 2 teeth (Z) and a maximal axial depth of cut $a_{p,max}$ of 20 mm. A total of three consecutive passes were performed on the sample's sides, each of which had an axial depth of cut a_p of 3 mm and a radial depth of cut a_e of 1 mm. At the end of the experimental tests, the tool did not show any sign of wear regarding ISO 8688-2.

For ductile materials such as metal, milling parameters can be experimentally determined using the Couple Tool-Material (CTM) standard NF E 66-520-6. Similarly, the CTM methodology was used to ensure that the tool is compatible with this polymeric material with or without CF use. In this work, the qualification test alone was performed since machining parameters for PLA are not known with this tool. To achieve this objective, starting parameters were selected from literature [10], picked to give the best results in terms of surface roughness after machining in dry conditions. Parameters were then increased and decreased by 20% around the starting value. Table 3 shows the experimental plan which was carried out twice: once in dry conditions (without using any CF) and once under pressurized air. A minimum of four repetitions were performed for each set of cutting conditions.

Table 3. Experimental plan.

Conditions category	v_c [m/min]	f_z [mm/tooth]
vc-	60.3	0.1
fz-	75.4	0.08
Baseline	75.4	0.1
fz+	75.4	0.12
vc+	90.5	0.1

2.3. Surface roughness and dimensions assessment

A Diavite DH-06 surface roughness meter was used to evaluate the arithmetic surface roughness R_a of the sample's exterior faces before and after machining. These values were assessed following the guidance of ISO 4288. After machining, surface roughness was assessed for three horizontal strips corresponding to the three passes performed while machining. In this study, the strips are referred to as 1 to 3, strip 1 being the first one machined. Along these strips, surface roughness was measured in three different zones to best cover the whole length of the strip (Fig. 1).

The samples width was measured before and after machining using a Wenzel LH54 Coordinate Measuring Machine (CMM) with a PH10M head and a spherical probe of 1.5 mm-diameter from Renishaw. The difference between width before and after machining operations was used to determine effective radial depth of cut $a_{e,eff}$, which differs from the theoretical value of a_e because of the inability to reach tight tolerances in MEX. Each measured length L (in mm) by the CMM had a measurement uncertainty (in µm) of $3 + L/300$ for the X and Y axes and $3.5 + L/300$ for the Z axis.

2.4. Cutting forces

The parts were clamped into a 3D-printed support, itself attached to a Type 9256C2 Kistler force sensor. The cutting forces signals were recorded thanks to a Kistler 5070A charge amplifier and Kistler 5697A2 data acquisition system linked to a computer executing the DynoWare software. The sampling frequency was set to 20 kHz.

Results were processed using a Butterworth low pass filter of order 4 with a cutoff frequency of 2500 Hz corresponding to half of the natural frequency of the Kistler force sensor. The Root Mean Square (RMS) value of the total cutting force F_{tot} of each pass was then computed from F_x, F_y and F_z components (equation 1) measured by the force sensor, which are proportional in classical models. Therefore, F_{tot} is proportional to the cutting force F_c in the v_c direction and is used as an image of the cutting power P_c as cutting forces in

the cutting and radial directions are proportional. Following the guidance of NF E 66-520-6 standard, the specific cutting energy W_c was determined using the total cutting force F_{tot} and the cutting cross section A_D following equation 1 involving the effective radial depth of cut $a_{e,eff}$ defined earlier:

$$W_c = \frac{F_{tot}}{A_D} \text{ with } F_{tot} = \sqrt{F_x^2 + F_y^2 + F_z^2} \text{ and } A_D = a_p \times a_{e,eff} \quad (1)$$

Regarding the tests where compressed air was used as CF, the force contribution to recorded forces of the airflow itself has been determined. The machining program was run five times on each machined side after a run of effective machining. The average contribution was then computed and subtracted from the recorded cutting forces in the cases for which CF was used, before computing the specific cutting energy W_c.

2.5. Temperature monitoring

During milling, temperatures were measured using an IQ-AAA Seek Thermal camera (Fig. 2) with a temperature accuracy of 5%. The temperature range of the camera went from 10°C to 300°C. The emissivity ε considered for this work was set to 0.78 according to Ferraris et al. [24]. The temperatures recorded in this study must therefore be considered as estimations.

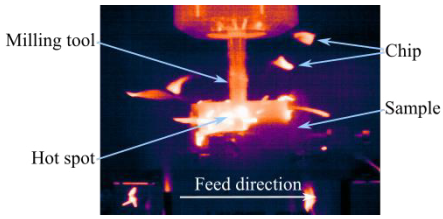

Fig. 2. Thermal camera image.

3. Results and Discussion

3.1. Samples visual assessment

Before measuring R_a, a visual examination of the samples was made to assess the presence of burr and torn areas. Indeed, in some conditions, areas can appear on the machined face, where material seems to have been pulled and torn rather than cut (Fig. 3).

Unlike the tearing phenomenon appearing only in certain cutting conditions, burr tends to form almost systematically during machining. No trend could be identified between burr formation and cutting conditions nor cutting temperatures. Burr forms in two zones: on the top face where chips seem to remain because they were not entirely cut, and on the side of the sample where the tool exits the material (Fig. 3). The latter should not cause an issue since, in the case of a continuous cut around a workpiece, the machining program can be lengthened to ensure that no exit burr remains. Regarding burr formation on the top face, the remaining chips that are not fully cut are fragile. Some of them can be cleared out by the pressurized air used as CF. However, more investigations should be conducted on how to prevent their formation.

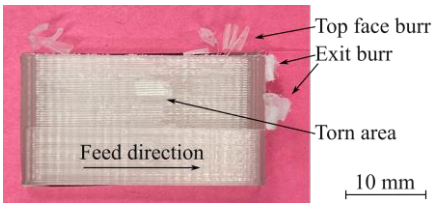

Fig. 3. Two types of burr formation.

3.2. Temperature monitoring

As mentioned by Dilberoglu et al. [15], reaching above glass transition temperature can result in inferior surface quality. Therefore, Table 4 shows the maximum recorded temperature for each of the cutting conditions which does not vary significantly between the different cutting parameters.

Table 4. Maximum cutting temperatures.

Conditions category	Without CF use [°C]	With CF use [°C]
vc-	92.1	70.4
fz-	93.9	70.9
Baseline	93.6	73.3
fz+	90.1	74.9
vc+	92.9	75.7

On the other hand, the maximum temperature during cutting decreases significantly with the use of CF, although temperatures still reach above the material glass transition temperature T_g (61°C). CF use can therefore help restrain potential heat damage.

Given the low depth of cut used in this study, there was not any case of chip fusion and wrapping around the tool, even with the reached temperatures.

3.3. Surface roughness analysis

Overall, surface roughness tends to vary considerably, going from 0.19 µm to over 10 µm. The best surface quality is obtained for the baseline case in dry conditions (Fig. 4): the mean surface roughness R_a reaches 1.24 µm and the dispersion over all the passes strips and zones is at its lowest compared to other cutting conditions. Furthermore, surfaces machined in these conditions do not show any sign of torn areas.

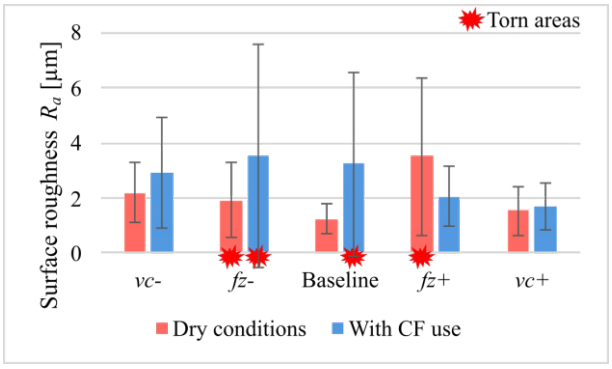

Fig. 4. Mean R_a depending on cutting conditions.

For dry conditions, variations around baseline parameters systematically increase surface roughness and dispersion. Thus, it suggests that these baseline conditions are an optimized operating point for this tool and material with the depths of cut defined previously.

The worst surface quality, showing the highest dispersion (σ = 4.06 µm) as well as the highest mean surface roughness value (R_a = 3.52 µm), is obtained in the *fz-* conditions using CF. For these cutting conditions, torn areas are almost systematically present on strips 1 and 3 but not on strip 2. Surface roughness of these torn areas vary considerably reaching values as low as 0.32 µm and as high as 13.93 µm, explaining such a high dispersion. Thanks to the absence of torn areas, the surface roughness of the second pass (Strip 2) reaches a low mean surface roughness R_a of 1.40 µm with low dispersion while it is not the case for strips 1 and 3 (Fig. 5).

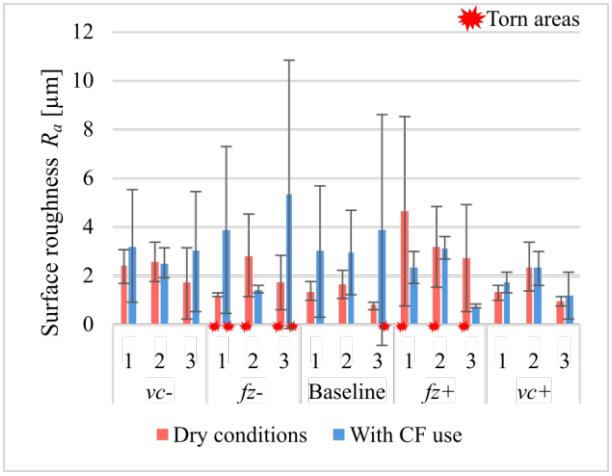

Fig. 5. Mean R_a depending on the pass strip and the cutting conditions.

For the case for which CF is used, surface roughness R_a and dispersion decrease from *fz-* conditions to *vc+* conditions. The optimized operating point seems to be moved towards higher cutting speeds. This is beneficial regarding productivity since higher cutting speed means less machining time. However, CF use does not seem to allow lower surface roughness than the values already achieved in dry conditions.

3.4. Cutting forces analysis

Overall, values of the specific cutting energy W_c and its dispersion (Fig. 6) follow the opposite trend of surface roughness values R_a and its dispersion. For instance, for the dry conditions case, baseline conditions show high values of W_c then decreases for other cutting conditions where R_a reached low values for baseline conditions and increased for the others. Furthermore, in the case of CF use, for *fz+* and *vc+* conditions, the surface roughness values R_a decreased which corresponds to increasing values of W_c.

Dispersion of W_c being an image of the cutting conditions stability, the machining process seems less stable while increasing the cutting speed v_c.

Finally, values of W_c are overall higher using CF than not using it. One explanation for this phenomenon is that the material softens more in dry conditions as the temperatures reached during machining are higher by around 20°C. In fact, for semicrystalline polymers such as PLA, crystalline domains slowly become amorphous around the glass transition temperature. Therefore, crystalline domains may still be present when CF is used.

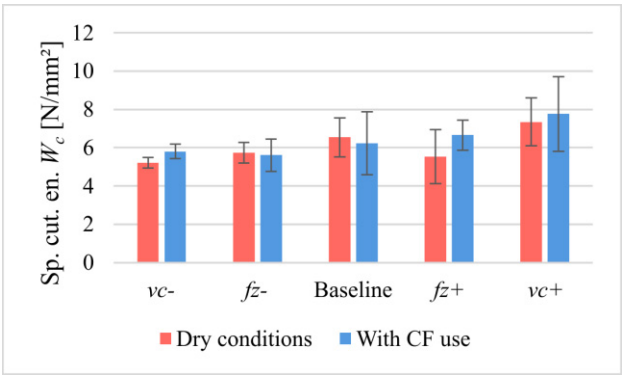

Fig. 6. Specific cutting energy W_c depending on the cutting conditions.

3.5. Cutting coefficients modeling

To tackle the lack of existing models for PLA machining, a usual cutting force model for metallic materials, developed by Rivière-Lorphèvre and Filippi [22], has been selected. To implement it, an inverse analysis is first performed on the measured data. The linear model is then used, which considers that the cutting forces along three directions of space dF_i (i being r, t, and a, for radial, tangential and the axial direction, respectively) are modeled as the product of the specific cutting pressure K_i by the undeformed chip thickness h and the axial depth of cut dA [22]. The equation linking the cutting forces and coefficient is therefore as follows:

$$dF_i = K_i \cdot h \cdot dA \text{ with } i = r, t, or\ a \quad (2)$$

On Fig. 7, the graph shows the simulated cutting forces compared to the measured ones over two revolutions of the cutting tool for the baseline case in dry conditions.

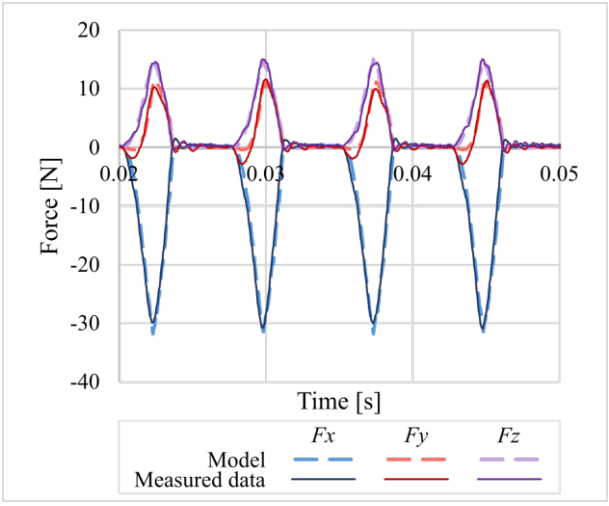

Fig. 7. Simulated cutting forces compared to measured ones for the baseline case in dry conditions.

The identified specific cutting pressures are as follows: K_t = 208 MPa, K_r = 57 MPa, and K_a = 95 MPa. The comparison between modeled and simulated forces shows a very good agreement, so much that the experimental and simulated curves cannot be easily distinguished in Fig. 7. This suggests that, using optimized cutting parameters, the linear model is relevant to model cutting forces in PLA machining.

4. Conclusions and Prospects

This study has demonstrated the impact of CF use on the finish milling of PLA FFF-obtained parts. Thermal properties of PLA, such as low thermal conductivity and low melting temperature, are a major challenge in the milling process. Key findings include:

- Best surface quality is achieved under baseline cutting conditions in dry conditions (R_a.= 1.24 µm).
- Burr formation was observed both using and not using CF with no clear trend linking to cutting conditions. Further research could be carried out on burr formation specifically as it is part of the final workpiece surface quality.
- Maximum cutting temperatures are decreased by the use of CF by approximately 20°C in this work configuration, helping to bring the material closer to its glass transition temperature but still exceeding it.
- The use of CF does not improve surface quality for the same cutting parameters as in dry conditions. Another operating point with increased cutting speed should exist for conditions with CF use which can help increase productivity.
- Dispersion of cutting forces follows an opposite trend to the surface roughness values leading to less stable process (higher dispersion) for a better surface quality reached.
- A mechanistic model designed for metallic materials has been implemented and shows very good agreement to the experimental data when using optimizing cutting parameters, therefore proving the relevance of the model.

Acknowledgements

The first author would like to thank Lorenzo Colantonio and Alexander Pizzaro Garcia for their precious help during the experimental tests.

This work was carried out within the Manufacturing 21 network, which gathers about 20 French research laboratories. The covered topics are the study and modeling of the manufacturing processes, especially machining and AM, as well as the emergence of new manufacturing methods.

References

[1] Pei E, Bernard A, Gu D, Klahn C, Monzón M, Petersen M, et al., editors. Springer Handbook of Additive Manufacturing. Cham: Springer International Publishing; 2023. https://doi.org/10.1007/978-3-031-20752-5.

[2] Gibson I, Rosen D, Stucker B, Khorasani M. Additive Manufacturing Technologies. Cham: Springer International Publishing; 2021. https://doi.org/10.1007/978-3-030-56127-7.

[3] Vyavahare S, Teraiya S, Panghal D, Kumar S. Fused deposition modelling: a review. Rapid Prototyp J 2019;26:176–201. https://doi.org/10.1108/RPJ-04-2019-0106.

[4] Lalegani Dezaki M, Mohd Ariffin MKA, Ismail MIS. Effects of CNC Machining on Surface Roughness in Fused Deposition Modelling (FDM) Products. Materials 2020;13:2608. https://doi.org/10.3390/ma13112608.

[5] Mertkan İA, Tezel T, Kovan V. Improving surface and dimensional quality with an additive manufacturing-based hybrid technique. Int J Adv Manuf Technol 2023;128:1957–63. https://doi.org/10.1007/s00170-023-12055-z.

[6] Kalia S, Avérous L. Biodegradable and Biobased Polymers for Environmental and Biomedical Applications. John Wiley & Sons; 2016.

[7] Li Y, Wang S, Qian S, Liu Z, Weng Y, Zhang Y. Depolymerization and Re/Upcycling of Biodegradable PLA Plastics. ACS Omega 2024;9:13509–21. https://doi.org/10.1021/acsomega.3c08674.

[8] Bhattacharya M, Reis RL, Correlo V, Boesel L. Material properties of biodegradable polymers. Biodegrad. Polym. Ind. Appl., Elsevier; 2005, p. 336–56. https://doi.org/10.1533/9781845690762.3.336.

[9] Lalegani Dezaki M, Mohd Ariffin MKA, Baharuddin BTHT. Experimental Study of Drilling 3D Printed Polylactic Acid (PLA) in FDM Process. In: Dave HK, Davim JP, editors. Fused Depos. Model. Based 3D Print., Cham: Springer International Publishing; 2021, p. 85–106. https://doi.org/10.1007/978-3-030-68024-4_5.

[10] Cloëz L, Fontaine M, Gilbin A, Barrière T. Machinability of PLA obtained by injection molding under a dry milling process, 2024, p. 1877–86. https://doi.org/10.21741/9781644903131-208.

[11] Lalegani Dezaki M, Mohd Ariffin MKA. Post-processing of FDM 3D-Printed Polylactic Acid Parts by CNC Trimming. In: Dave HK, Davim JP, editors. Fused Depos. Model. Based 3D Print., Cham: Springer International Publishing; 2021, p. 195–212. https://doi.org/10.1007/978-3-030-68024-4_11.

[12] Mehtedi ME, Buonadonna P, Carta M, Mohtadi RE, Marongiu G, Loi G, et al. Effects of milling parameters on roughness and burr formation in 3D- printed PLA components. Procedia Comput Sci 2023;217:1560–9. https://doi.org/10.1016/j.procs.2022.12.356.

[13] Kartal F, Kaptan A. EXPERIMENTAL DETERMINATION OF THE OPTIMUM CUTTING TOOL FOR CNC MILLING OF 3D PRINTED PLA PARTS. Int J 3D Print Technol Digit Ind 2023;7:150–60. https://doi.org/10.46519/ij3dptdi.1267634.

[14] Pămărac RG, Petruse RE. Study Regarding the Optimal Milling Parameters for Finishing 3D Printed Parts from ABS and PLA Materials. Acta Univ Cibiniensis Tech Ser 2018;70:66–72.

[15] Dilberoglu UM, Yaman U, Dolen M. A comprehensive guide to milling techniques for smoothing the surfaces of 3D-printed thermoplastic parts. Rapid Prototyp J 2024;30:1648–62. https://doi.org/10.1108/RPJ-08-2023-0277.

[16] Dessarthe A. Usinage des polymères. Trav Matér - Assem 2000. https://doi.org/10.51257/a-v1-bm7426.

[17] Zmeskal O, Marackova L, Lapcikova T, Mencik P, Prikryl R. Thermal properties of samples prepared from polylactic acid by 3D printing. AIP Conf Proc 2020;2305:020022. https://doi.org/10.1063/5.0033857.

[18] Zhang A, Li Y. Thermal Conductivity of Aluminum Alloys—A Review. Materials 2023;16:2972. https://doi.org/10.3390/ma16082972.

[19] Boschetto A, Bottini L, Veniali F. Finishing of Fused Deposition Modeling parts by CNC machining. Robot Comput-Integr Manuf 2016;41:92–101. https://doi.org/10.1016/j.rcim.2016.03.004.

[20] Arrazola PJ, Özel T, Umbrello D, Davies M, Jawahir IS. Recent advances in modelling of metal machining processes. CIRP Ann 2013;62:695–718. https://doi.org/10.1016/j.cirp.2013.05.006.

[21] Wan M, Li S-E, Yuan H, Zhang W-H. Cutting force modelling in machining of fiber-reinforced polymer matrix composites (PMCs): A review. Compos Part Appl Sci Manuf 2019;117:34–55. https://doi.org/10.1016/j.compositesa.2018.11.003.

[22] Rivière-Lorphèvre E, Filippi E. Mechanistic cutting force model parameters evaluation in milling taking cutter radial runout into account. Int J Adv Manuf Technol 2009;45:8–15. https://doi.org/10.1007/s00170-009-1943-9.

[23] Nanovia. Nanovia PLA EF 3D850 : Sans perturbateur endocrinien : Nanovia. Nanovia - Compos Mater Adv Ind n.d. https://nanovia.tech/en/ref/pla-ef/ (accessed June 10, 2024).

[24] Ferraris E, Zhang J, Van Hooreweder B. Thermography based in-process monitoring of Fused Filament Fabrication of polymeric parts. CIRP Ann 2019;68:213–6. https://doi.org/10.1016/j.cirp.2019.04.123.